Regenerative Therapy 25 (2024) 290–301

Contents lists available at ScienceDirect

Regenerative Therapy

journal homepage: http://www.elsevier.com/locate/reth

Original Article

circ-Amotl1 in extracellular vesicles derived from ADSCs improves wound healing by upregulating SPARC translation

Dazhou Wu, Shengyi Chen, Dongdong Huang, Zhipeng Huang, Na Zhen, Zhenxu Zhou, Jicai Chen*

Department of Hernia and Abdominal Wall Surgery, The First Affiliated Hospital of Wenzhou Medical University, PR China

ARTICLE INFO

Article history:
Received 24 August 2023
Received in revised form
26 December 2023
Accepted 18 January 2024

Keywords:
ADSC-Evs
circ-Amotl1
IGF2BP2
SPARC
Wound healing

ABSTRACT

Aim: This study aims to explore the mechanism of circ- AMOT-like protein 1 (Amotl1) in extracellular vesicles (Evs) derived from adipose-derived stromal cells (ADSCs) regulating SPARC translation in wound healing process.

Methods: The morphology, wound healing rate of the wounds and Ki67 positive rate in mouse wound healing models were assessed by H&E staining and immunohistochemistry (IHC). The binding of IGF2BP2 and SPARC was verified by RNA pull-down. Adipose-derived stromal cells (ADSCs) were isolated and verified. The Evs from ADSCs (ADSC-Evs) were analyzed.

Results: Overexpression of SPARC can promote the wound healing process in mouse models. IGF2BP2 can elevate SPARC expression to promote the proliferation and migration of HSFs. circ-Amotl1 in ADSC-Evs can increase SPARC expression by binding IGF2BP2 to promote the proliferation and migration of HSFs.

Conclusion: ADSC-Evs derived circ-Amotl1 can bind IGF2BP2 to increase SPARC expression and further promote wound healing process.

1. Introduction

Wound healing is a vital physiological process that can maintain the integrity of skin following trauma and it is a complex, multifaceted process in human or animal involving hemostasis/inflammation, proliferation, and remodeling [1]. This healing process also involves multiple cell types in the wound region or systemic system [2]. Fibroblasts, a major cell type in the dermis, can synthesize and deposit structural proteins including collagen and elastin that can be assembled into the extracellular matrix (ECM) [3]. Skin fibroblasts carry differentially expressed genes essential for the synthesis, proliferation, and migration of ECM, which are fundamental processes during wound healing [4]. A negative feedback loop between fibroblast proliferation and ECM production is an important mechanism for dermal maturation, which can restore tissue homeostasis after wound healing [5]. Owing to the complexity of the wound healing process, the molecular mechanisms involved in this study remain poorly understood. Hence, it is significant to pay more attention to the molecules related to fibroblast proliferation and ECM.

Secreted protein acidic and rich in cysteine (SPARC), also known as osteonectin or BM-40, is a prototype of the biologically active glycoprotein family that can bind to cells as well as to ECM components [6]. A prior study has reported a promoting role of SPARC in fibroblast migration, which facilitates granulation tissue formation, contributing to wound repair [7]. This may be related to the promotion of endothelial angiogenesis upon activation of its relatives such as SPARC related modular calcium binding 1 (SMOC1) [8]. circ-AMOT-like protein 1 (Amotl1), a circular form of AMOTL1, has been recently revealed to serve as a contributor to cardiac repair [9]. Furthermore, ectopic expression of circ-Amotl1 accelerates wound healing, which provides new insight into the development of clinical strategies for skin wound healing [10]. Human insulin-like growth factor 2 (IGF2) mRNA binding proteins 2 (IGF2BP2) is an m6A reader that involves in the development and progression of multiple human diseases by interacting with long non-coding RNAs (lncRNAs), microRNAs (miRNAs), mRNAs, etc. [11]. Given the

* Corresponding author. Department of Hernia and Abdominal Wall Surgery, The First Affiliated Hospital of Wenzhou Medical University, Shangcai County, South Baixiang Street, Ouhai District, Wenzhou city, Zhejiang Province, 325000, PR China.
E-mail address: cjc60321@163.com (J. Chen).

Peer review under responsibility of the Japanese Society for Regenerative Medicine.

https://doi.org/10.1016/j.reth.2024.01.005

binding relations between IGF2BP2 and SPARC as well as between circ-Amotl1 and IGF2BP2 found in our bioinformatics analysis using SRAMP and Starbase database, we speculated whether there existed a circ-Amotl1/IGF2BP2/SPARC axis involving the wound healing process.

Cell therapy, especially the application of adipose-derived stromal cells (ADSCs), has emerged as a promising therapeutic option for the refractory chronic wounds due to their regenerative capability [12]. ADSCs can enhance reepithelialization and angiogenesis to participate in dermal wound healing in both physiological and pathological settings [13]. During wound healing, cultured ADSCs can affect multiple processes, such as angiogenesis, inflammation, and ECM remodeling, through a plethora of regenerative growth factors and immune mediators [14]. Recently, extracellular vesicles (Evs) derived from ADSCs have shown great potential to enhance diabetic wound healing through cell-to-cell communication mechanisms [15]. Evs are cell-created vesicles of 40–100 nm in diameter carrying cargoes such as small non-coding RNAs, proteins, etc. and can transmit these molecules to target cells [16]. In the current study, *in vitro* and in vivo experiments were carried out to investigate whether ADSC-Evs derived circ-Amotl1 can regulate wound healing through mediating IGF2BP2 and SPARC.

2. Materials and methods

2.1. Bioinformatics analysis

GSE168760 (skin tissues: untreated group vs. laser ablation treatment group) and GSE181022 (skin tissues: adults vs. infants) datasets were processed from GEO database (https://www.ncbi.nlm.nih.gov/geo/) for analysis. The differential expressed genes shared in both datasets were screened using Venn diagram. The target genes of SPARC were predicted in SRAMP database (https://www.cuilab.cn/sramp) and the binding sites were predicted by Starbase (http://starbase.sysu.edu.cn/). PathCards (https://pathcards.genecards.org/pathcards) was used to predict the signal pathways related to SPARC.

2.2. Wound healing mouse models

C57BL mice aged 4 weeks were purchased from Hunan Silaikejingda Experimental Animal Co., Ltd and housed in specific pathogen-free conditions with the temperature of 26~28 °C and humidity of 50~65 %. All mouse experiments were designed according to ethical guidelines and approved by ethical committee of The First Affiliated Hospital of Wenzhou Medical University. A full-thickness wound was made on the back of each mouse using a 5 mm Miltex® Biopsy Punch with Plunger. The wound area was calculated by measuring the maximized length × maximized width. After 12 days, mice received euthanasia and the wound tissues were collected. The back of each mouse was injected with 200 μL solution (1.4×10^9 particles/mL) [17], and mice were accordingly classified into Control (no treatment), Evs (injected with Evs), Evs-shNC (injected with negative control), Evs-shcirc-Amotl1 (injected with shcirc-Amotl1 Evs), oe-NC (injected with control plasmid) and oe-SPARC (injected with oe-SPARC plasmid) groups, with ten mice in each group. Overexpression vector and shRNA vector were purchased from GenePharma (Shanghai, China).

2.3. Western blot

The total protein in tissues and cells was extracted using RIPA cell lysis buffer (R0010, Solarbio) according to the instructions. The samples were subjected to cell lysis at 4 °C for 15 min before centrifugation at 15,000 g for 15 min. Then the supernatant was collected using a BCA kit (20201ES76, Yeasen biotechnology, Shanghai) and the protein concentration of each sample was detected. The protein was quantified based on concentration and then separated using polyacrylamide gel electrophoresis, after which the protein was transferred into the PVDF membrane and blocked with 5 % BSA at room temperature for 1 h. Primary rabbit antibodies, including IGF2BP2 (1:1000, abcam, ab124930), SPARC (1:1000, abcam, ab207743), MMP2 (1:1000, abcam, ab92536), MMP9 (1:500, abcam, ab76003), Notch1 (1:1000, abcam, ab52627), Collagen I (1:1000, abcam ab138492), Collagen III (1:1000, abcam ab184993), Jagged1 (1:500, abcam, ab109536), Hes1 (1:1000, abcam, ab108937), GAPDH (1:10,000, abcam, ab8245) were diluted and incubated with the protein at a shaking table for overnight at 4 °C. The membranes were washed in TBST for 5 min × 3 times and the HRP labeled goat anti-rabbit IgG (ab205718, 1:20,000, Abcam, Cambridge, UK) dilutions were added for incubation at room temperature for 1 h. The membranes were then washed with TBST for 5 min × 3 times and reacted with color-developing liquid. The quantification was analyzed using ImageJ 1.48 (National Institutes of Health) using the ratio of the grey value of the target protein with GAPDH. Each experiment was conducted three times.

2.4. H&E staining

The skin tissues were fixed in 4 % paraformaldehyde solution and dehydrated for paraffin section with each slice of 5 μm for H&E staining. Tissues were observed under a microscope.

2.5. Immunohistochemistry

Sections (4 μm) were routinely deparaffinised and treated with endogenous peroxidase for 10 min at room temperature, followed by washing in distilled water 2 × 3 times. Then 0.01 M sodium citrate buffer (pH 6.0) was added for heating in a microwave oven to boil. After boiling, the microwave was turned off for 5–10 min and this process was repeated 1–2 times. The PBS (pH 7.3) cooled sections were added 5 % BSA blocking solution dropwise for 20 min at room temperature. The excess liquid was removed and the sections were incubated with 30 μl of KI67 primary antibody (1:100, Abbkine, USA) at 37 °C for 1 h, after that the sections were washed with PBS (pH 7.3) 2 × 3 times and incubated with biotinylated goat anti-rabbit IgG for 20 min at 37 °C. Being further washed with PBS (pH 7.3) 2 × 3 times, the sections were added SABC at 37 °C for 20 min, followed by PBS washing 5 × 4 times. DAB color development kit was used for color development. Then 1 mL of distilled water was taken out and one drop was respectively added into reagent A, B and C in the kit before the sections were added. The reaction was terminated by slices washing with distilled water after color development at room temperature. Hematoxylin was used for re-staining. Sections were dehydrated, transparentized, and sealed. The positive rate of KI67 was calculated under a microscope.

2.6. RNA pull-down

HSF cells were transfected with biotin-labeled RNA biotin-labeled IGF2BP2 using Lipofectamine 2000 (Invitrogen) based on instructions. After transfection for 48 h, cells were collected and washed in PBS. Then cells were incubated with specific cell lysis buffer (Ambion, Austin, Texas, USA) for 10 min, after which 50 mL cell lysis buffer was packaged and the rest of the buffer was incubated with RNase-free/Yeast tRNA (Sigma, St. Louis, MO, USA) coated M–280 Streptavidin magnetic beads (Sigma, St. Louis, MO, USA) for 3 h at 4 °C. Cell was then washed twice with cold lysis buffer, thrice with low salt buffer (0.01 mol/L ph7.2 PBS) and once

with high salt buffer (0.05 mol/L ph7.2 PBS) before RNA was extracted using the Trizol method for quantitative reverse transcription polymerase chain reaction (qRT-PCR). IgG was used as the control.

2.7. Actinomycin D assay

The cell culture medium was added 2 mg/mL Actinomycin D (sigma-aldrich, StLouis, MO, USA) with DMSO as the negative control. After Actinomycin D treatment, the SPARC mRNA expression in each group was detected using RT-PCR.

2.8. qRT-PCR

Total RNA was extracted based on the instructions of Trizol (Invitrogen, Car, USA) and treated with PrimeScript RT kit (RR037A, Takara, Japan) for reverse transcription into cDNA. SYBR®Premix ExTaqTMII kit (RR820A, TaKaRa) was used for quantitative PCR according to instructions and the PCR apparatus system (ABI 7500, ABI, Foster City, CA, USA) was used for PCR reaction. The relative expression of target genes was calculated using GAPDH as the internal control and $2^{-\Delta\Delta Ct}$ method [18]. Each experiment was repeated three times. $\Delta\Delta Ct = \Delta Ct_{\text{experimental group}} - \Delta Ct_{\text{control group}}$, $\Delta Ct = Ct_{\text{target gene}} - Ct_{\text{internal control}}$. The primer sequences were designed by Sangon (Shanghai, China) (Table 1).

2.9. CCK8 assay

Cells were cultured in a 96-well plate. CCK-8 solution (10 μl, Dojindo, Japan) was added to each well for incubation at 37 °C for 1–3 days based on the instructions of manufacturer. A microplate reader (Thermo, USA) measured the optical density at 450 nm.

2.10. Cell scratch assay

Human Skin fibroblasts (HSFs) were seeded in a 12-well plate and cultured at 37 °C till the coverage of 80 %. A 10 μL pipette tip was used to make a scratch in the culture medium. Then the cells were further cultured at 37 °C for 24 h before a microscope (Nikon Eclipse Ti, Nikon, Japan) was used to observe the cell migration ability.

2.11. Transwell assay

The transwell chamber was coated with 50 μL Matrigel gel (Sigma, USA) and HSFs at the logarithmic phase were starved for 24 h and digested on the next day to make the concentration of 2×10^5/mL. Then 0.2 mL cell suspension was added in the upper chamber, while 700 μL culture medium contained 10 % FBS in the lower chamber. The Transwell chamber was incubated at 37 °C with 5 % CO_2 for 24 h. After that, the upper chamber was removed, and the lower chamber was fixed in methyl alcohol for staining with 0.1 % crystal violet aqueous solution. An inverted microscope (XDS-800D, Shanghai, Caikon Optical Instrument Co., LTD, China) was used to count cell numbers. Five random views were selected, in which cell number was counted and averaged.

Table 1
Primer sequences for quantitative reverse transcription polymerase chain reaction.

Gene	Sequence
circ-Amotl1-F	5'- ATGCTCCACGAGATGGTCAAG- -3
circ-Amotl1-R	5'- ACTACTGGGGCTATAACAAGCAG-3'
Collagen I–F	5′ - CCTGGATGCCATCAAAGTCT- -3′
Collagen I -R	5′- AATCCA TCGGTCATGCTCTC -3′
Collagen III–F	5′- GGA GAGTCCATGGATGGTGG -3′
Collagen III–R	5′- TTTGCTCCA TTCCCCAGTGT -3′
GAPDH-F	F:5′- AATCCCATCACCATCTTC -3′
GAPDH-R	R:5′- AGGCTGTTGTCATACTTC -3′

F, forward; R, reverse.

2.12. Isolation and identification of adipose-derived stem cells (ADSCs)

ADSCs were isolated from adipose tissues and cultured in MEM-O (Gibco, Grand Island, NY, USA) containing 10 % FBS at 3000 cells per cm. Cells were then treated with 0.25 % trypsin–EDTA and washed with DPBS. The cell stocks of passage four were used for further experiments [19].

ADSCs were cultured in FBS-free endothelial cell culture medium (Gibco, Grand Island, NY, USA) and after cell culture for two days, Evs derived from ADSCs (ADSC-Evs) were extracted using differential centrifugation method. The simplified steps include 10 min of centrifugation at 300×*g* for 10 min, with the supernatant being collected; 10 min of centrifugation at 2000×*g* for 10 min, with the supernatant being collected; CP100NX centrifuge at 10,000×*g* for 30 min, with the supernatant being collected; 90 min of centrifugation at 100,000×*g* at 4 °C, with the supernatant being removed; the precipitates were re-suspended in PBS and centrifuged at 100,000×*g* for 90 min. The purity of Evs was improved after resuspension in PBS.

2.13. Identification of ADSC-Evs

Nanosight particle size analysis: 20 μg Evs were dissolved in 1 mL PBS and whirled for 1 min. Nanosight LM10 particle size analysis apprentice (NTA, Malvern instrument, UK) was used to observe the distribution of Evs.

Transmission electron microscope (TEM): 20 μL ultracentrifuged Evs were loaded into a carbon-coated microscope copper gridding for 2 min and then received negative staining with phosphotungstic acid solution (12,501-23-4, Sigma–Aldrich, USA) for 5 min. The gridding was washed in PBS three times to remove the excessive phosphotungstic acid solution and half-dried with filter paper. The Evs were observed under a Hitachi TEM (H7650, Japan) at 80 KV.

Western blot was applied to detect the expressions of biomarkers of Evs. The condensed Evs suspension was measured for protein concentration using a BCA kit (23,227, Thermofisher, USA). Sodium dodecyl sulfate polyacrylamide gel electrophoresis (SDS-PAGE) gel was prepared for protein denature and electrophoresis. After the protein was transferred into the membrane, the expressions of CD9 (ab236630, abcam), CD63 (ab134045, abcam), CD81 (ab92726, abcam) and Calnexin (ab92573, abcam) were detected.

2.14. Uptaking of EVs

PKH67 green fluorescence kit (Sigma–Aldrich, USA) was used to label the purified Evs. The labeled Evs were resuspended in 1 mL Diluent C solution and 4 μL PKH67 ethanol dye solution was added in 1 mL Diluent C for preparation of 4×10^{-6} M dye solution. Then the 1 mL Evs suspension was mixed with the dying solution for 5 min and 2 mL 1 % extracellular Evs were incubated with PBS for 1 min to terminate the dying. The Evs were pelleted by ultracentrifugation at 100, 000×*g* for 2 h to enable a sucrose density of 1.13–1.19 g/mL for enrichment to collect the Evs [20]. PKH67 labeled Evs were incubated with HSFs at 37 °C for 12 h, after which the HSFs were fixed with 4%PFA and washed with PBS before the cell nucleus was stained with DAPI (sigma, D9542, USA). The uptakes of Evs by HSFs were observed under a fluorescence

microscope (ECLIPSE E800, Nikon, Japan). HSFs were purchased from ATCC.

Evs were isolated from 300 μL ADSCs conditioned culture medium (Gibco, Grand Island, NY, USA). circ-Amotl1 was labeled with FITC and FITC-circ-Amotl1 was packaged into Evs using electroporation. Specifically, 400 μL electroporation solution (21 % Optiprep, 25 mm KCl, 100 mm potassium phosphate, pH 7.2) was added 30 uL FITC- circ-Amotl1 and 200 ng Evs in 4 mm electroporation tube (Eppendorf, Hauppauge, NY). The Evs received electroporation using a E2510 electroporation instrument (Eppendorf, Hauppauge, NY) at 0–2000 v and maintained for 5 min at 4 °C. The unreacted circ-Amotl1 was removed by PBS washing, FITC-circ-Amotl1 (green) and Dil-labeled Evs were incubated with HSFs for 48 h. The locations of FITC and Dil were observed under a fluorescence microscope (ECLIPSE E800, Nikon, Japan).

2.15. Co-culture

Culture medium (control group), ADSCs conditioned culture medium (Gibco, Grand Island, NY, USA, ADSC-CM group), ADSC-Evs (ADSC-Evs group) or complete culture medium of ADSCs without Evs (ADSC-Evs-del group) was cultured with HSFs to detect the expressions of Evs biomarkers, Amotl1, IGF2BP2 and SPARC.

2.16. Statistical analysis

All data were processed by GraphPad Prism 8.0 (GraphPad Software, La Jolla, CA, USA). Each experiment was repeated for at least 3 times. Measurement data were expressed as mean ± standard deviation (Mean ± SD). Unpaired T-test was used for comparison between two groups, while one-way ANOVA was used for analysis among multiple groups, with Tukey's test as post hoc test. Two-way ANOVA or repeated measures analysis of variance was applied for comparisons among multiple groups or multiple time points, with Tukey's test as post hoc test. P value of less than 0.05 was regarded as having statistical significance.

3. Results

3.1. SPARC activates Notch signal pathway to promote wound healing process through ECM remodeling

To identify the key regulator of wound healing, GSE168760 and GSE181022 datasets were screened from GEO database. Differential analysis on GSE168760 found 32 differentially expressed genes and 47 differentially expressed genes in GSE181022. The overlap of differentially expressed genes of the two datasets is shown in the Venn diagram (Fig. 1A). A total of 4 differentially expressed genes were shared by the two datasets, including OL5A2, COL1A1, SPARC and COL5A1. Laser ablation treatment is the gold standard for skin regeneration. GSE168760 dataset displayed the differentially expressed SPARC after laser ablation treatment, while GSE181022 dataset demonstrated that differentially expressed SPARC between adults and infants. SPARC was highly expressed in both GSE168760 and GSE181022 datasets (Fig. 1B and C).

To explore the function of SPARC on wound healing process, a 5 mm wound was made on both sides of the back area in a mouse model. On the next modeling day, plasmid with SPARC overexpression was injected into the wound area. The detection on the wound healing process showed that the expression of SPARC in oe-SPARC group was significantly elevated compared with oe-NC group (Fig. 1D). Observation on the wound area and wound healing rate showed that the wound area in oe-SPARC group was smaller and the wound healing rate in oe-SPARC group was much faster than those in oe-NC group (Fig. 1E and F). H&E staining showed the regeneration rate of epithelial tissues in oe-SPARC group was increased and the scar width was decreased compared with those in oe-NC group (Fig. 1G). Immunohistochemistry detecting Ki67 positive rate showed the Ki67 rate in oe-SPARC group was elevated in contrast to that in oe-NC group (Fig. 1H). Those results suggested overexpression of SPARC can promote wound healing process.

Data in PathCards supported the implication of SPARC in ECM remodeling and Notch signal pathway (Fig. 1I). Moreover, ECM remodeling and Notch signal pathway were proven to regulate wound healing process (J. [21,22]). Western blot measured the related proteins of ECM remodeling and Notch signal pathway, and manifested that oe-SPARC group had decreased expressions of MMP2 and MMP9, and elevated expressions of Notch1, Jagged1 and Hes1, compared with those in oe-NC group (Fig. 1J). The above results showed that overexpression of SPARC can suppress MMP-2 and MMP-9 expression to increase ECM remodeling and activate Notch signal pathway to promote wound healing process.

3.2. IGF2BP2 elevates SPARC expression by increasing SPARC mRNA stability

SRAMP predicted the m6A modification sites of SPARC (Fig. 2A). IGF2BP2 is an m6A reading protein which can increase mRNA stability and translation by recognizing m6A sites. Starbase found the binding sites of IGF2BP2 and SPARC mRNA (Fig. 2B). To determine the possible regulation of IGF2BP2 on SPARC expression, IGF2BP2 was overexpressed and then the SPARC expression was detected. The results showed that oe-IGF2BP2 group had increased expressions of IGF2BP2 and SPARC compared with oe-NC group (Fig. 2C and D). RNA pull-down showed increased SPARC mRNA can be pulled down in oe-IGF2BP2 group in contrast to that in oe-NC group (Fig. 2E). Detection of SPARC mRNA stability showed that compared with oe-NC group, the SPARC mRNA stability was increased in oe-IGF2BP2 group (Fig. 2F). Those results showed that IGF2BP2 can increase SPARC mRNA stability to elevate SPARC expression.

3.3. IGF2BP2 promotes the proliferation and migration of HSFs by increasing SPARC expression

Evidence in a previous study showed IGF2BP2 can increase wound healing by enhancing cell migration [23]. To explore the role of IGF2BP2/SPARC axis in the wound healing process, oe-IGF2BP2 or oe-IGF2BP2+sh-SPARC was transfected into HSFs. qRT-PCR and western blot showed that compared with oe-NC + sh-NC group, oe-IGF2BP2+sh-NC group had increased expressions of IGF2BP2 and SPARC, while compared with oe-IGF2BP2+sh-NC group, oe-IGF2BP2+sh-SPARC group had decreased expression of SPARC (Fig. 3A and B). CCK8 assay, cell scratch and Transwell assay showed that cell proliferation and migration ability in oe-IGF2BP2+sh-NC group was increased compared with oe-NC + sh-NC group, but decreased in oe-IGF2BP2+sh-SPARC group when compared with oe-IGF2BP2+sh-NC group (Fig. 3C–E). qRT-PCR demonstrated that compared with oe-NC + sh-NC group, the expressions of Collagen I and Collagen III were increased in oe-IGF2BP2+sh-NC group, but decreased in oe-IGF2BP2+sh-SPARC group when contrast to those in oe-IGF2BP2+sh-NC group (Fig. 3F and G). Those results showed that IGF2BP2 can regulate SPARC expression to increase the proliferation and migration of HSFs.

3.4. ADSCs-derived circ-Amotl1 can bind IGF2BP2 to increase SPARC expression

ADSC-Evs were found to wound healing process [24]. To determine the implication of IGF2BP2/SPARC axis derived from ADSCs

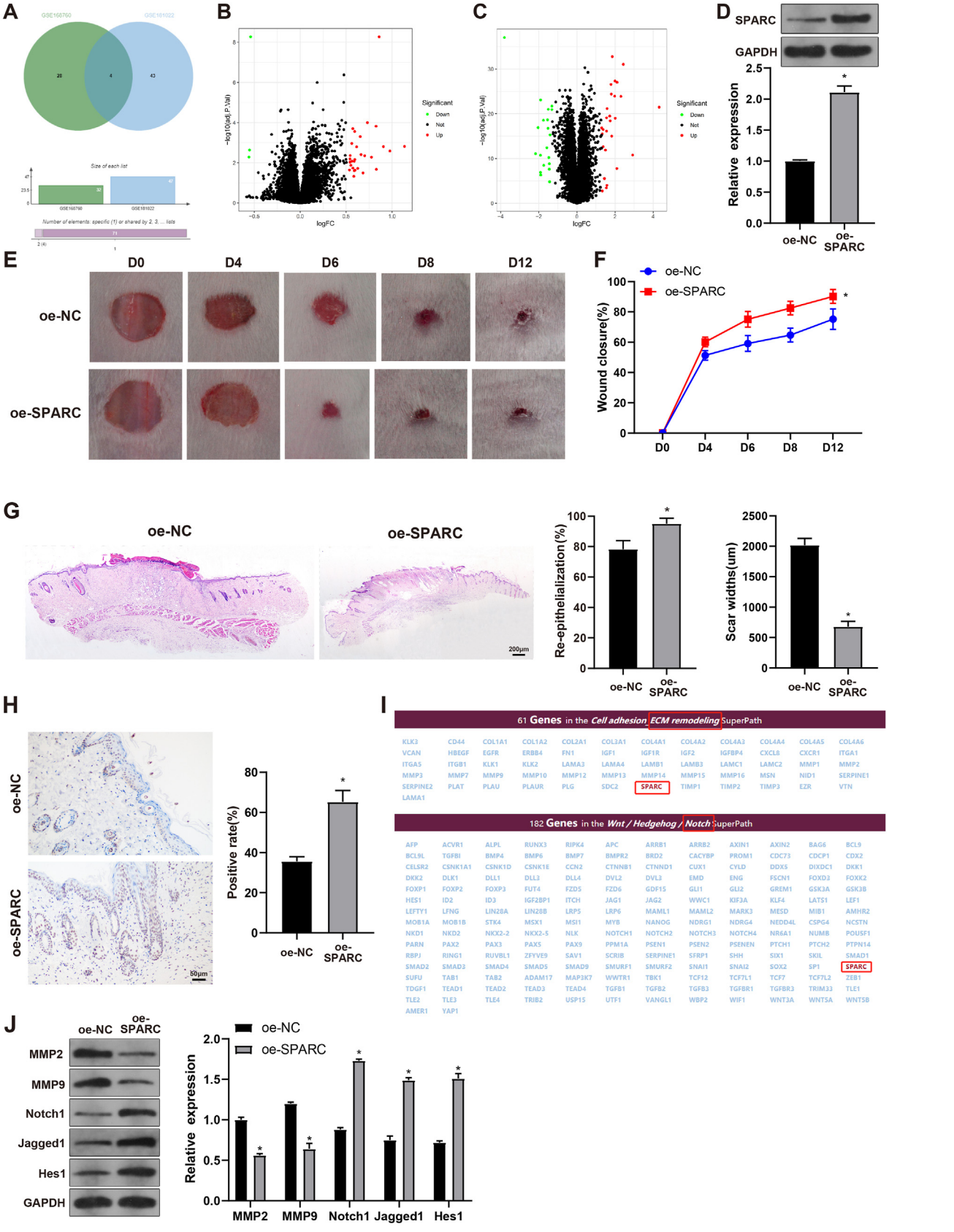

Fig. 1. SPARC regulates ECM remodeling to activate Notch signal pathway to promote wound healing process A, Overlaps of differential expressed genes in both GSE168760 and GSE181022 datasets; B, differential expressed genes in GSE168760; C, differential expressed genes in GSE181022; D, SPARC expression detected by western blot; E, wound healing area in each group; F, wound healing rate in each group; G, H&E staining on epithelial tissues; H, Immunohistochemistry detected the positive expression of Ki67; I, PathCards supported the implication of SPARC in ECM remodeling and Notch signal pathway; J, western blot detecting the expressions of MMP2, MMP9, Notch1, Jagged1 and Hes1. Data were expressed as mean ± standard deviation (SD). Comparison between two groups was analyzed using independent sample *t* test, n = 10. Cellular experiment was conducted for 3 times. *, compared with oe-NC group, $P < 0.05$. ECM, extracellular matrix.

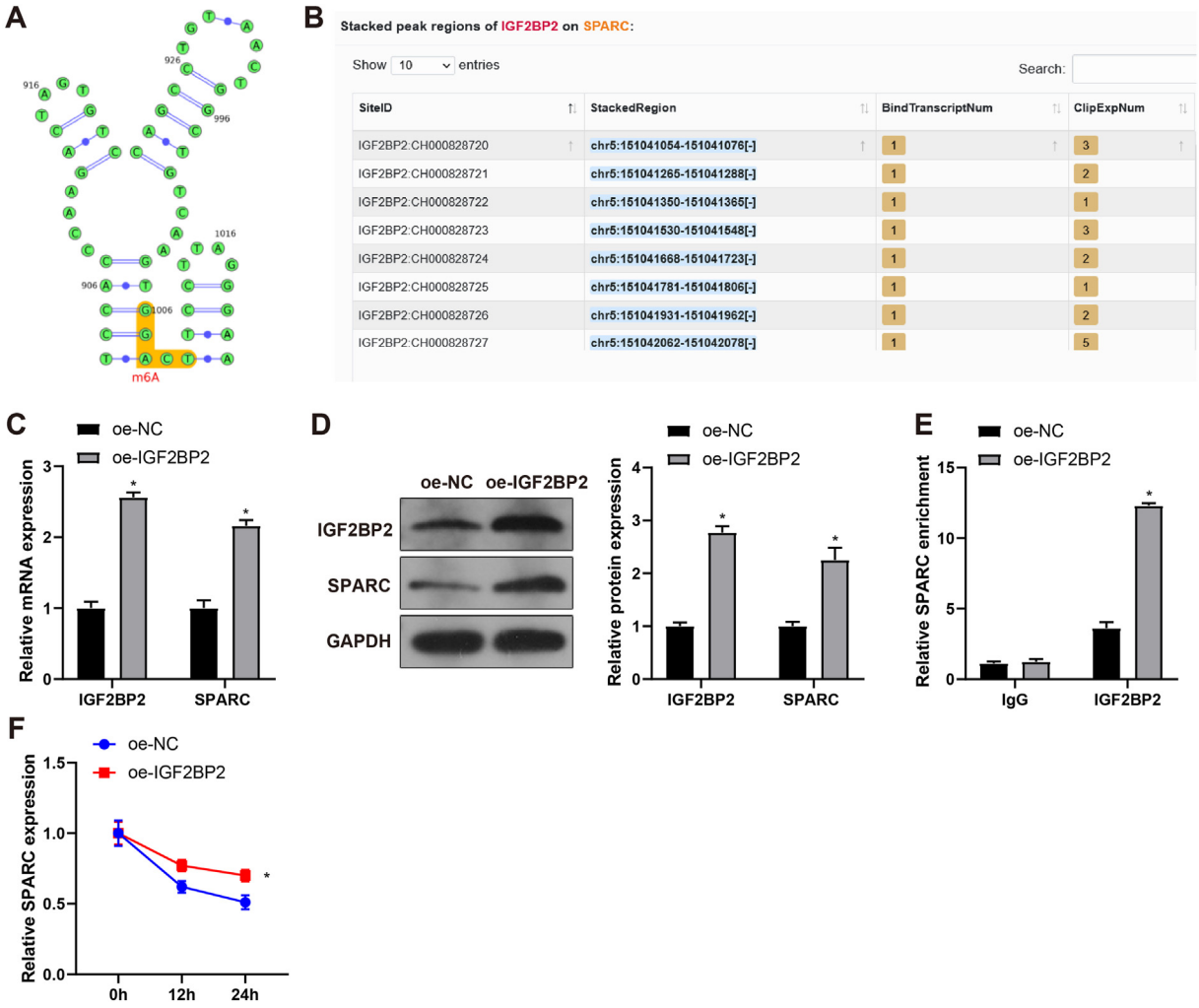

Fig. 2. IGF2BP2 increases SPARC expression by elevating SPARC mRNA stability A, SRAMP database predicted m6A modification sites of SPARC; B, Starbase predicted the binding sites of IGF2BP2 and SPARC mRNA; C, qRT-PCR detected the mRNA expressions of IGF2BP2 and SPARC; D, western blot detected the protein expressions of IGF2BP2 and SPARC; E, RNA pull down detected the SPARC mRNA level pulled down by IGF2BP2; F, Actinomycin D detected SPARC mRNA stability. Data were expressed as mean ± standard deviation (SD). Comparison between two groups was analyzed using independent sample *t* test, n = 10. Cellular experiment was conducted for 3 times. *, compared with oe-NC group, $P < 0.05$.

derived Evs in wound healing, the extracted ADSCs and ADSC-Evs were identified. The isolated ADSCs showed cells in long shuttle shape and grown in clones (Fig. 4A). Flow cytometry showed enrichment of ADSC biomarkers, CD44, CD90 and CD105 (Fig. 4B), suggesting ADSCs were successfully isolated. ADSC-Evs were isolated from the supernatant of ADSCs culture medium. TEM and NTA demonstrated that the isolated ADSC-Evs were double-packaged vesicles at 30–120 nm (Fig. 4C and D). Western blot detecting the expressions of Evs biomarkers CD9, CD63 and CD81 showed that the protein expressions of CD9, CD63 and CD81 were significantly enhanced, but no expression of cytoplasmic endoplasmic reticulum protein Calnexin was detected (Fig. 4E).

Then PKH67 labeled ADSC-Evs were cultured with HSFs for 12 h before fixation and photographing. The results showed that a large proportion of ADSC-Evs entered HSFs and located around the cell nucleus, while PBS treated HSFs showed no green fluorescence (Fig. 4F). Those results showed that HSFs can internalize ADSC-Evs.

Starbase predicted the binding of circ-Amotl1 and IGFBP2 (Fig. 4G) and data from a previous study showed that circ-Amotl1 can enhance the wound repairing process [10]. RNA pull-down assay found enriched circ-Amotl1 in oe-IGF2BP2 group instead of oe-NC group (Fig. 4H). To identify the transference of circ-Amotl1, we transfected FITC-circ-Amotl1 into Evs and the Evs were labeled with Dil for incubation with HSFs for 48 h. The co-location of FITC and Dil in HSFs showed that HSFs internalize the Evs, which contains circ-Amotl1 (Fig. 4I). Western blot and qRT-PCR detected the circ-Amotl1 and biomarkers of Evs expressions in HSFs, which showed that compared with HSFs in control group, HSFs in ADSC-CM group had elevated expressions of CD9, CD63, CD81 and circ-Amotl1, while compared with that HSFs in ADSC-Evs group, HSFs in ADSC-Evs-del group had decreased expressions of CD9, CD63, CD81 and circ-Amotl1 (Fig. 4J and K). Western blot showed that compared with control group, HSFs in ADSC-CM group had elevated expressions of IGF2BP2 and SPARC, while compared with HSFs cultured with ADSC-Evs, HSFs in ADSC-Evs-del group had decreased expressions of IGF2BP2 and SPARC (Fig. 4J). Those results showed that circ-Amotl1 derived from ADSC-Evs can bind IGF2BP2 to increase SPARC expression.

3.5. circ-Amotl1 in ADSC-Evs can bind IGF2BP2 to increase SPARC expression to promote proliferation and migration of HSFs

HSFs were cultured with ADSC-Evs or circ-Amotl1 depleted ADSC-Evs, in which the expression of circ-Amotl1 was detected by

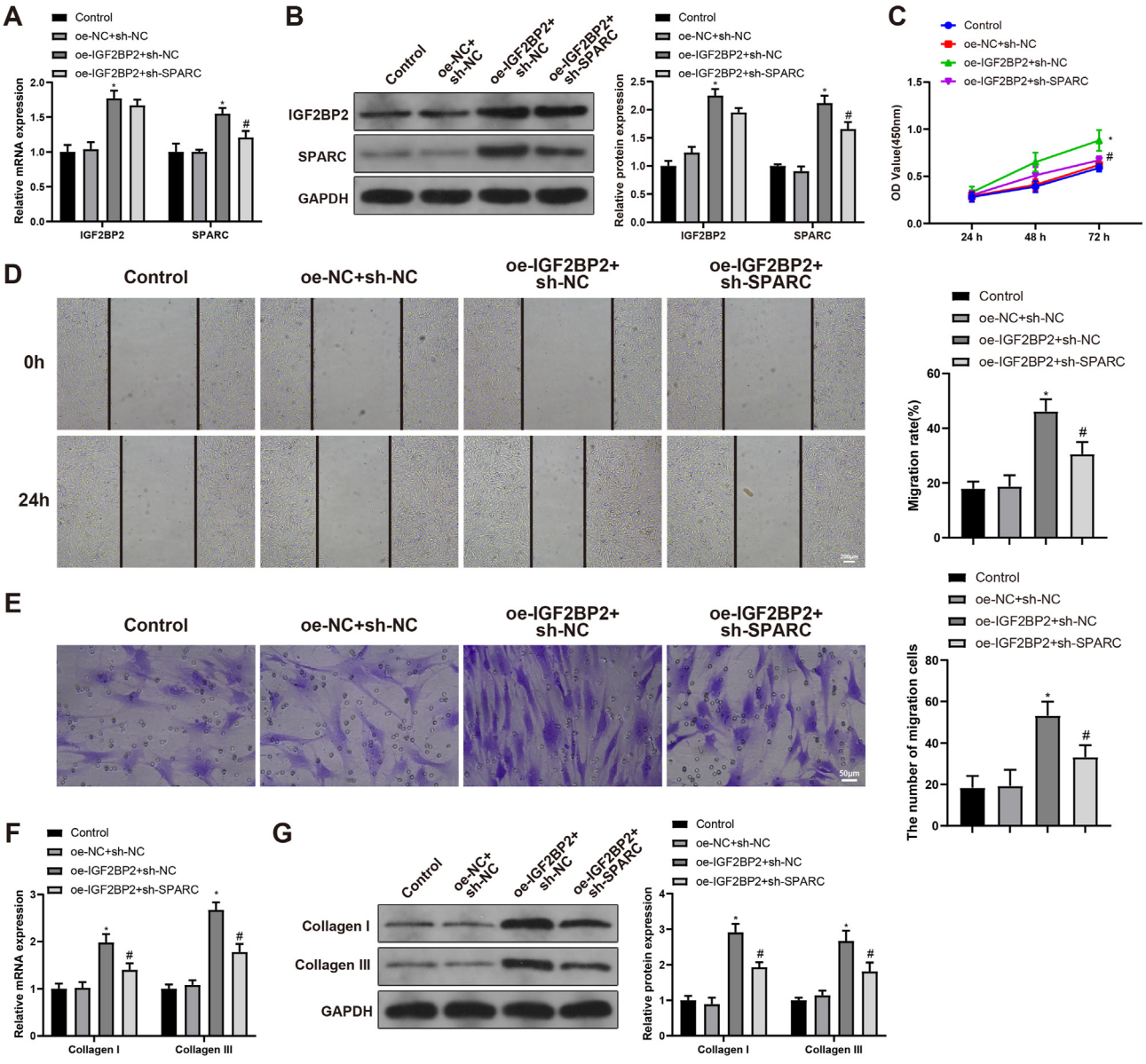

Fig. 3. IGF2BP2 can regulate SPARC expression to increase the proliferation and migration of HSFs. A, qRT-PCR detected the mRNA expressions of IGF2BP2 and SPARC; B, western blot detected the protein expressions of IGF2BP2 and SPARC; C, CCK8 assay measured cell proliferation ability; D, cell scratch measured cell migration ability; E, Transwell measured cell migration ability; F, qRT-PCR detected the expressions of Collagen I and Collagen III; G, western blot detected the protein expressions of Collagen I and Collagen III. Data were expressed as mean ± standard deviation (SD). Comparison among three groups was analyzed using one-way ANOVA. Analysis on data among multiple time points were conducted by repeated ANOVA, with Bonferroni as post hoc analysis. Cellular experiment was conducted for 3 times. *, compared with oe-NC + sh-NC group, $P < 0.05$. #, compared with oe-IGF2BP2+sh-NC group, $P < 0.05$.

qRT-PCR. The results showed that after the depletion of circ-Amotl1 in ADSCs, the expression of circ-Amotl1 in ADSC-Evs was decreased (Fig. 5A). ADSC-Evs were cultured with HSFs and then qRT-PCR was used to detect the expression of circ-Amotl1 in HSFs. Compared with control group, HSFs cultured with Evs had increased expression of circ-Amotl1, while compared with Evs-shNC group, the expression of circ-Amotl1 in Evs-shcirc-Amotl1 group was significantly reduced (Fig. 5B). Western blot showed that compared with control group, HSFs cultured with Evs had elevated expressions of IGF2BP2 and SPARC, while compared with Evs-shNC group, the Evs-shcirc-Amotl1 group had reduced expressions of IGF2BP2 and SPARC (Fig. 5C). CCK8, cell scratch and Transwell assay showed that HSFs cultured with Evs had enhanced cell proliferation and migration ability compared with control group. In contrast, HSFs in Evs-shcirc-Amotl1 group had suppressed proliferation and migration ability compared with Evs-shNC group (Fig. 5D). qRT-PCR detection showed the expressions of Collagen I and Collagen III were increased in HSFs cultured with Evs, but decreased in Evs-shcirc-Amotl1, respectively compared with control group and Evs-shNC group (Fig. 5E–H). The above results showed circ-Amotl1 in ADSC-Evs increases SPARC expression through binding IGF2BP2 to enhance proliferation and migration of HSFs.

3.6. circ-Amotl1 in ADSC-Evs regulates IGF2BP2/SPARC axis to promote wound healing process

To clarify the regulation of ADSC-Evs derived circ-Amotl1 in IGF2BP2/SPARC axis in vivo, a 5 mm wound was made on the back

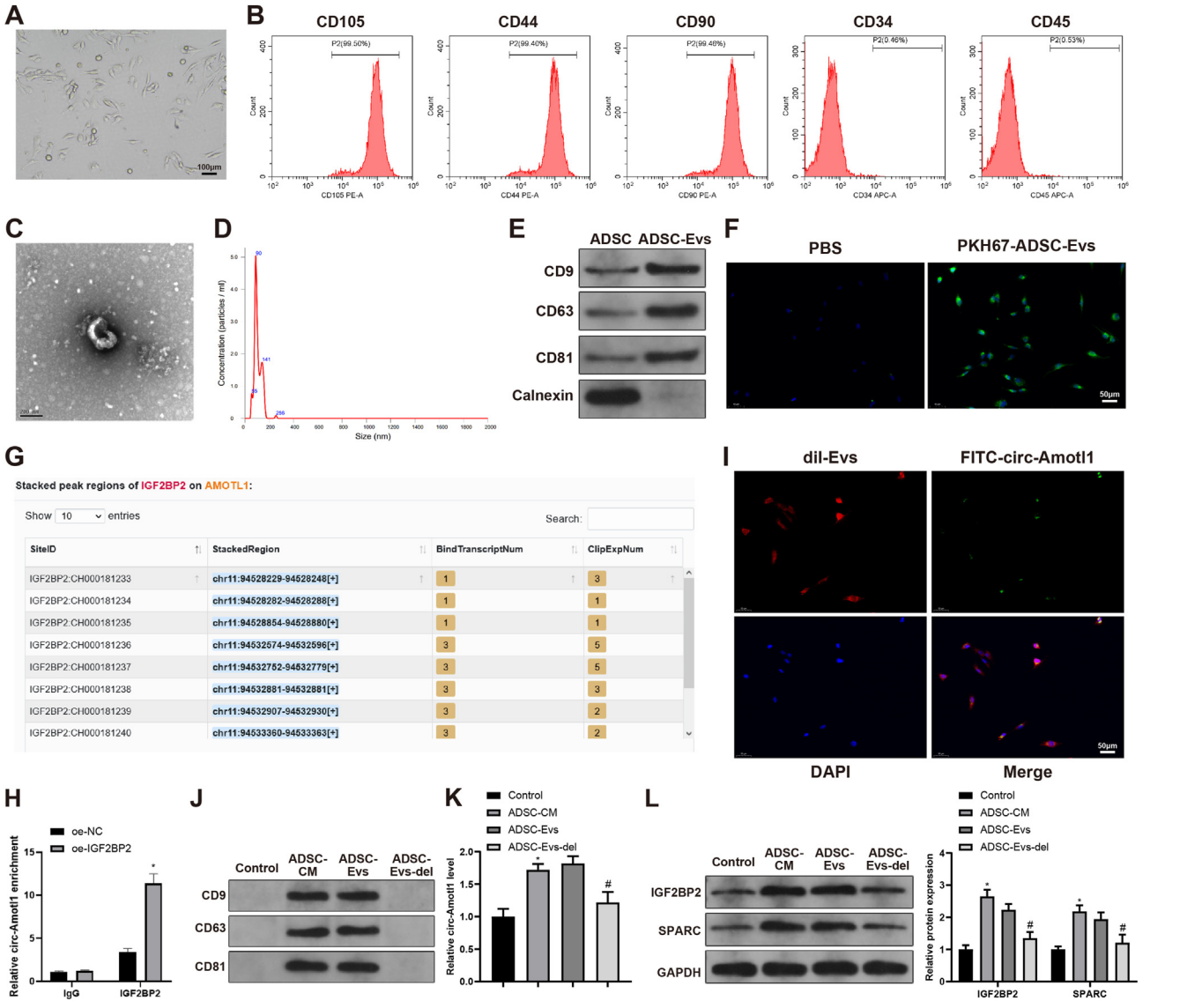

Fig. 4. circ-Amotl1 derived from ADSCs can bind IGF2BP2 to increase SPARC expression A, inverted microscope observed the morphology of ADSCs derived from adipocytes; B, ADSCs were identified by flow cytometry; C-D, TEM and NTA analyzed Evs; E, Western Blot detected the biomarkers of Evs; F, PKH67 fluorescence detected ADSC-Evs; G, Starbase predicted the binding of circ-Amotl1 and IGFBP2; H, RNA pull down verified the binding of circ-Amotl1 with IGFBP2; I, Immunofluorescence co-localization analysis detected the expression of circ-Amotl1; J, western blot detected the expressions of Evs biomarkers; K, qRT-PCR detected the expression of circ-Amotl1 in cultured HSFs; L, western blot detected the expressions of IGF2BP2 and SPARC; Data were expressed as mean ± standard deviation (SD). Comparison between two groups was analyzed using independent sample T test. Comparison among three groups was analyzed using one-way ANOVA, n = 10. Cellular experiment was conducted for 3 times.*, compared with Control group, $P < 0.05$ (CM: culture medium; del: depletion); ADSCs, adipose-derived stromal cells; Evs, extracellular vesicle; TEM, transmission electron microscopy; NTA, nanoparticle tracking analysis.

of mice. The wound healing process of mice was observed and recorded. qRT-PCR and western blot showed that the expressions of circ-Amotl1, IGF2BP2 and SPARC in Evs group were increased but decreased in Evs-shcirc-Amotl1 group, respectively compared with those in control group and Evs-shNC group (Fig. 6A and B). H&E staining and immunohistochemistry showed that mice in Evs group had faster wound healing rate, shorter scar width and increased Ki67 expression than those in control group, while mice in Evs-shcirc-Amotl1 group had a much slower wound healing rate, wider scar width and decreased Ki67 expression than those in Evs-shNC group (Fig. 6C–F). Those results demonstrated that circ-Amotl1 in ADSC-Evs can promote wound healing in mice through regulating IGF2BP2/SPARC axis.

4. Discussion

This study validated the therapeutic effect of ADSC-Evs on skin wound healing in a mouse model. Additionally, the present study proposed a novel mechanism that ADSC-Evs transmitted circ-Amotl1 to HSFs, which bound to IGF2BP2 to up-regulate SPARC, thereby accelerating the proliferation of HSFs. The results obtained here collectively demonstrated that ADSC-Evs carrying circ-Amotl1 could promote wound repair through regulating the IGF2BP2/SPARC axis.

At first, SPARC was demonstrated to expedite skin wound healing through ECM remodeling and Notch signaling pathway activation, which was partly consistent with the finding of a recent

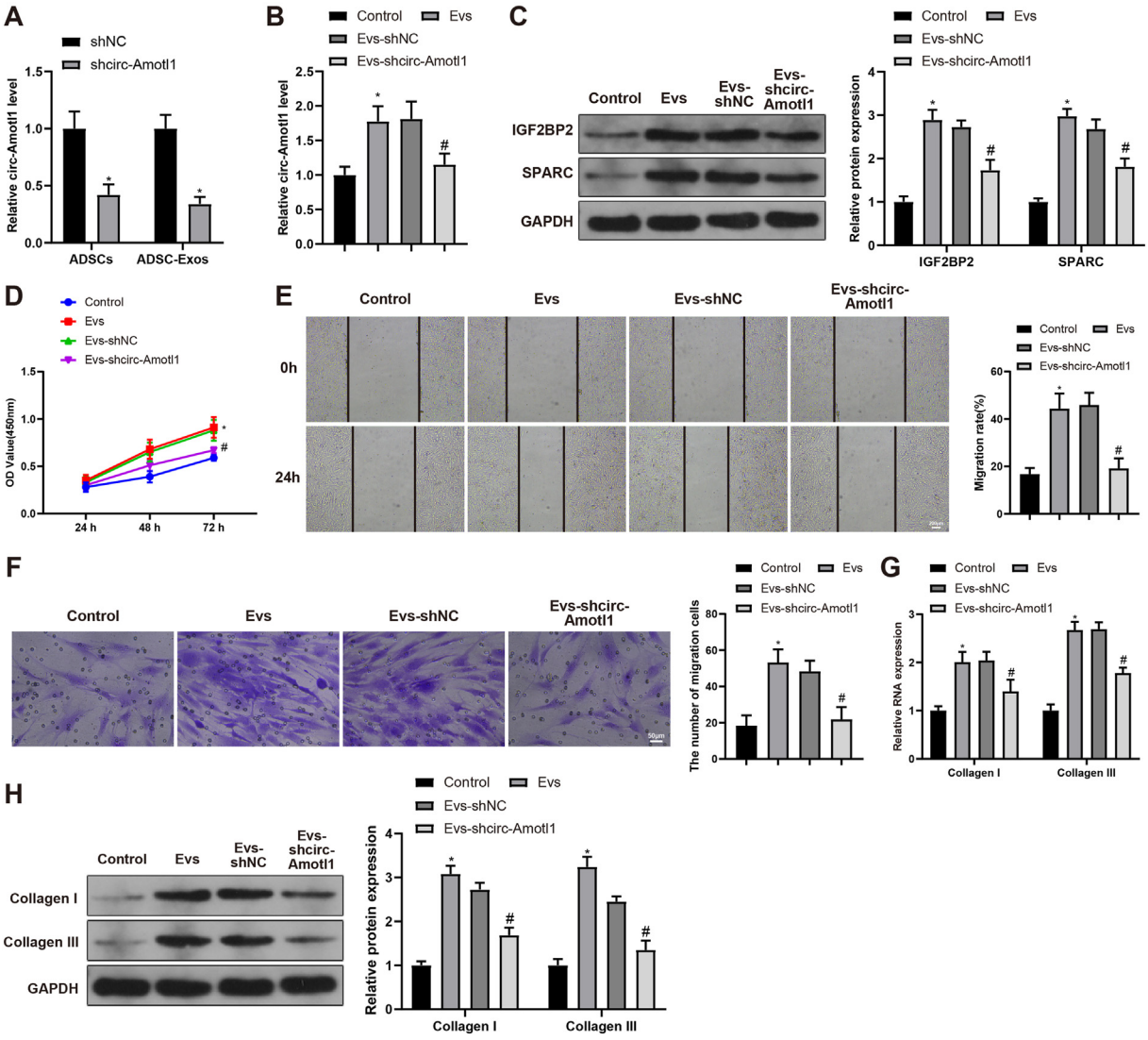

Fig. 5. circ-Amotl1 in ADSC-Evs increases SPARC expression through binding IGF2BP2 to enhance proliferation and migration of HSFs. A, qRT-PCR detected the expression circ-Amotl1 in ADSCs and ADSC-Evs; B, qRT-PCR detected the expression of circ-Amotl1 in HSFs; C, western blot detected the expression of IGF2BP2 and SPARC; D, CCK8 detected cell proliferation ability; E, cell scratch assay detected cell migration ability; F:Transwell assay detected cell migration ability; G, qRT-PCR detected the expressions of Collagen I and Collagen III; H, western blot detected the expressions of Collagen I and Collagen III. Data were expressed as mean ± standard deviation (SD). Comparison among three groups was analyzed using one-way ANOVA. Analysis on data among multiple time points were conducted by repeated ANOVA, with Bonferroni as post hoc analysis. Cellular experiment was conducted for 3 times.*, compared with Control group or sh-NC group, $P < 0.05$; #, compared with Evs-shNC group, $P < 0.05$.

study that exogenous SPARC can enhance limbal epithelial stem cell proliferation as well as the migration of the proliferating cells to facilitate wound repair [25]. SPARC is one of the key matricellular glycoproteins that are categorized primarily on the basis of functional criteria. These proteins are self-assembled into ECM fibrils and also orchestrate ECM properties by interacting with structural ECM proteins, growth factors, and even cells [26]. Dysregulation of ECM is implicated in the pathogenesis of wound healing-associated skin disorders (J. [21]), while activation of the Notch signaling pathway has been revealed to participate in the promotion of wound repair [22]. From the PathCards database, SPARC participated in ECM remodeling and regulation of the Notch signaling pathway. Ectopic expression of SPARC resulted in reductions in the levels of MMP-2 and MMP-9 as well as elevations in the levels of Notch1, Jagged1, and Hes1, suggesting the inhibitory effect of SPARC on ECM remodeling and promoting effect on the Notch signaling pathway activation.

Through SRAMP analysis, we found that multiple m6A modification sites existed on SPARC gene. A binding site between IGF2BP2 and SPARC was found based on the data from Starbase. IGF2BP2 is one of RNA-binding proteins with conserved m6A-binding domains to specifically recognize m6A modifcations; IGF2BPs can enhance the stability and storage of the target mRNAs in an m6A-dependent fashion in the normal and stress contexts (H. [27]). Based on the results of RNA pull-down assay and actinomycin-D test, this paper newly identified that IGF2BP2 could bind SPARC and increase the stability of SPARC. SPARC silencing reversed the promoting impacts of IGF2BP2 on HSF proliferation and migration, partly suggesting their correlation *in vitro*. Furthermore, this study revealed that circ-Amotl1 could bind to the m6A reader IGF2BP2 to increase the expression of SPARC. Several studies have widely reported circ-Amotl1 as a tumorigenic circular RNAs (circRNAs) in several tumors such as oral squamous cell carcinoma, breast tumors, and cervical tumors [28–30], but its role in wound healing remains

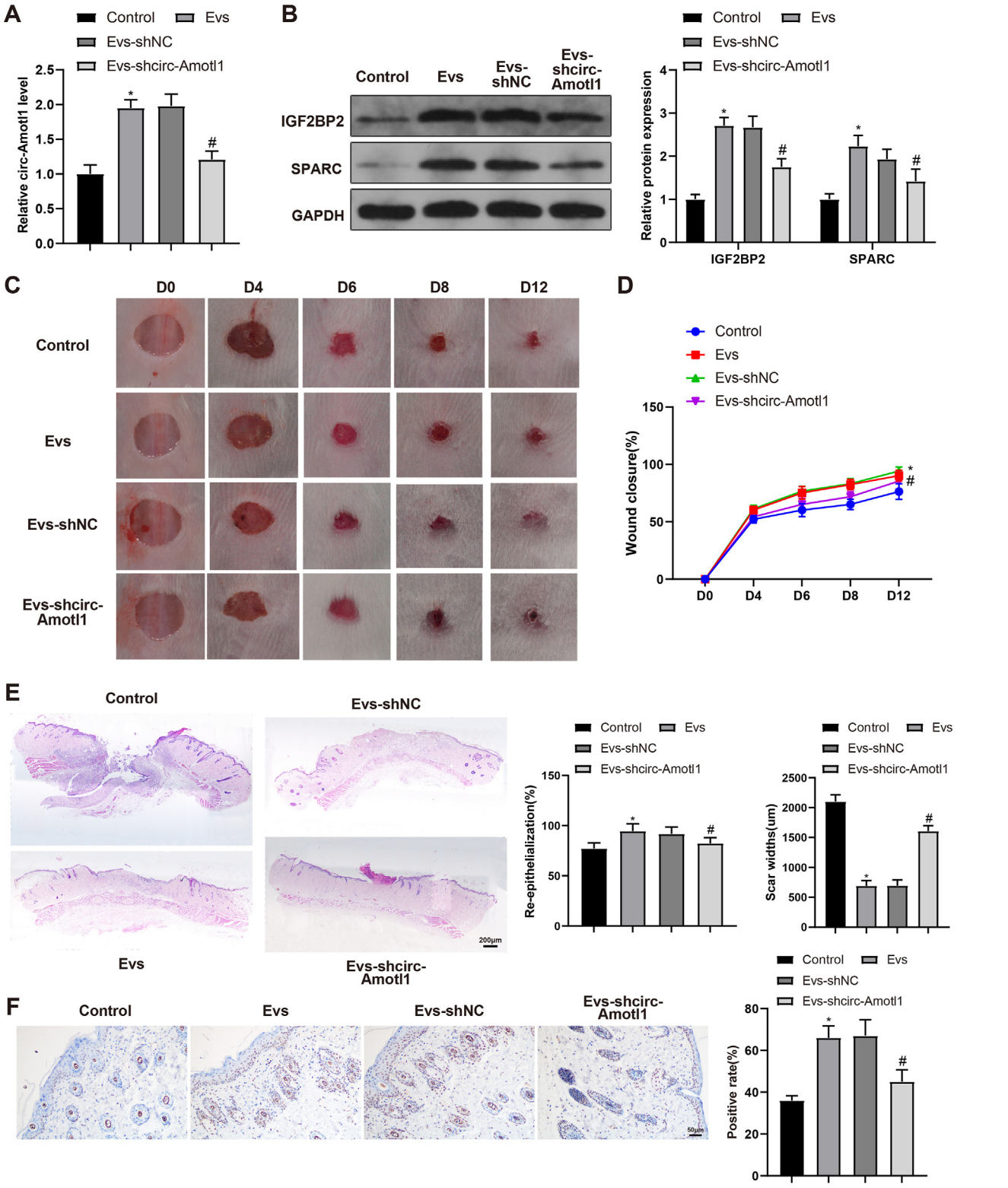

Fig. 6. circ-Amotl1 in ADSC-Evs can promote wound healing in mice through regulating IGF2BP2/SPARC axis. A, qRT-PCR detected the expression of circ-Amotl1; B, western blot detected the protein expressions of IGF2BP2 and SPARC; C, wound healing process in each group; D, comparison on wound healing rate in each group; E, H&E staining to observe the scar width; F, immunohistochemistry to detect the positive expression of Ki67. Data were expressed as mean ± standard deviation (SD). Comparison between two groups was analyzed using independent sample *t* test. Comparison among three groups was analyzed using one-way ANOVA. Analysis on data among multiple time points was conducted by one-way ANOVA, n = 10. Cellular experiment was conducted for 3 times. Experiment was conducted for 3 times.*, compared with Control group, $P < 0.05$; #, compared with Evs-shNC group, $P < 0.05$.

poorly understood. An existing study has suggested that circ-Amotl1 can physically bind to both PDK1 and AKT1 and then increase the nuclear translocation of pAKT, contributing to cardioprotection [9]. Besides, circ-Amotl1 can increase the nuclear translocation of STAT3 *via* regulating Dnmt3a and miR-17, as a mechanism responsible for skin wound repair [10], suggesting the significance of circ-Amotl1 in wound healing. On one hand, m6A can modify the function of circRNAs. On the other hand, circRNAs can regulate m6A *via* mediating the expression of m6A writers, erasers, and readers or affect the function of themselves [31]. Although the relationship between circ-Amotl1 and is not mentioned in previous studies, our study offered evidence supporting the regulatory effect of circ-Amotl1 on IGF2BP2.

Finally, the results of animal experiments demonstrated accelerated skin wound healing, increased re-epithelialization rate, decreased scar width, and increased Ki67 positive rate (corresponding to cell proliferation) in the wounded mice treated with ADSC-Evs. These results indicated the promoting role of ADSC-Evs in wound healing. ADSCs can release growth factors such as VEGF, TGF-β1, HGF, KGF, SDF-1, IL-8, and IL-6 during the proliferation period, thus enhancing angiogenesis, re-epithelialization, neovascularization, collagen synthesis, as well as skin cell proliferation [13]. More importantly, ADSC-Evs exert pro-proliferative, promigratory, and pro-angiogenic effects on keratinocytes, fibroblasts, and endothelial cells, shedding light on their promise as a therapeutic option for wound healing [15]. Another study also reported that human ADSC-Evs can accelerate angiogenesis in healing process, which might be related to exosomal EGR-1/lncRNA-SENCR/DKC1/VEGF-A signaling pathway [32]. *In vitro* experiments showed that loss of circ-Amotl1 ADSC-Evs in reduced the proliferation and migration of HSFs as well as the contents of collagen I and collagen III, which reversed the effect of ADSC-Evs on HSFs. *In vivo* evidence was also provided that ADSC-Evs promoted wound repair through delivering circ-Amotl1. Hence, we revealed a novel circ-Amotl1/IGF2BP2/SPARC axis involved in the therapeutic effect of ADSC-Evs on wound healing.

Taken together, this study provided an experimental basis for the application of ADSC-Evs in wound healing strategies clinically. Moreover, our study highlighted a molecular mechanism underlying the therapeutic activity of ADSC-Evs, wherein circ-Amotl1 upregulated SPARC through binding to an m6A reader IGF2BP2. However, more evidence is necessary to validate this mechanism in the following studies.

Funding

This research is funded by of Science Foundation of Zhejiang Province (Y20H030043) and Wenzhou Science & Technology Bureau (2023Y1149).

Data availability statement

All data are accessible upon reasonable request to the corresponding author.

Declaration of competing interest

The authors declare no conflict of interest.

Acknowledgments

Funding from the Science Foundation of Zhejiang Province (Y20H030043) and Wenzhou Science and Technology Bureau Foundation (Y2023464) is gratefully acknowledged.

References

[1] Wang PH, Huang BS, Horng HC, Yeh CC, Chen YJ. Wound healing. J Chin Med Assoc 2018;81(2):94–101. https://doi.org/10.1016/j.jcma.2017.11.002.
[2] Eming SA, Martin P, Tomic-Canic M. Wound repair and regeneration: mechanisms, signaling, and translation. Sci Transl Med 2014;6(265). https://doi.org/10.1126/scitranslmed.3009337. 265sr266.
[3] Ganier C, Rognoni E, Goss G, Lynch M, Watt FM. Fibroblast Heterogeneity in Healthy and wounded skin. Cold Spring Harbor Perspect Biol 2022;14(6). https://doi.org/10.1101/cshperspect.a041238.
[4] Rodrigues M, Kosaric N, Bonham CA, Gurtner GC. Wound healing: a cellular perspective. Physiol Rev 2019;99(1):665–706. https://doi.org/10.1152/physrev.00067.2017.
[5] Rognoni E, Pisco AO, Hiratsuka T, Sipila KH, Belmonte JM, Mobasseri SA, et al. Fibroblast state switching orchestrates dermal maturation and wound healing. Mol Syst Biol 2018;14(8):e8174. https://doi.org/10.15252/msb.20178174.
[6] Svoboda KKH, Gordon MK. Extracellular matrix: the proteins that function throughout the body. Anat Rec 2020;303(6):1509–13. https://doi.org/10.1002/ar.24404.
[7] Basu A, Kligman LH, Samulewicz SJ, Howe CC. Impaired wound healing in mice deficient in a matricellular protein SPARC (osteonectin, BM-40). BMC Cell Biol 2001;2:15. https://doi.org/10.1186/1471-2121-2-15.
[8] Luo MJ, Rao SS, Tan YJ, Yin H, Hu XK, Zhang Y, et al. Fasting before or after wound injury accelerates wound healing through the activation of pro-angiogenic SMOC1 and SCG2. Theranostics 2020;10(8):3779–92. https://doi.org/10.7150/thno.44115.
[9] Zeng Y, Du WW, Wu Y, Yang Z, Awan FM, Li X, et al. A circular RNA binds to and activates AKT phosphorylation and nuclear localization reducing apoptosis and enhancing cardiac repair. Theranostics 2017;7(16):3842–55. https://doi.org/10.7150/thno.19764.
[10] Yang ZG, Awan FM, Du WW, Zeng Y, Lyu J, Wu D, et al. The circular RNA interacts with STAT3, increasing its nuclear translocation and wound repair by modulating Dnmt3a and miR-17 function. Mol Ther 2017;25(9):2062–74. https://doi.org/10.1016/j.ymthe.2017.05.022.
[11] Wang J, Chen L, Qiang P. The role of IGF2BP2, an m6A reader gene, in human metabolic diseases and cancers. Cancer Cell Int 2021;21(1):99. https://doi.org/10.1186/s12935-021-01799-x.
[12] Brembilla NC, Vuagnat H, Boehncke WH, Krause KH, Preynat-Seauve O. Adipose-derived stromal cells for chronic wounds: scientific evidence and roadmap toward clinical practice. Stem Cells Transl Med 2023;12(1):17–25. https://doi.org/10.1093/stcltm/szac081.
[13] Goodarzi P, Alavi-Moghadam S, Sarvari M, Tayanloo Beik A, Falahzadeh K, Aghayan H, et al. Adipose tissue-derived stromal cells for wound healing. Adv Exp Med Biol 2018;1119:133–49. https://doi.org/10.1007/5584_2018_220.
[14] van Dongen JA, Harmsen MC, van der Lei B, Stevens HP. Augmentation of dermal wound healing by adipose tissue-derived stromal cells (ASC). Bioengineering (Basel) 2018;5(4). https://doi.org/10.3390/bioengineering5040091.
[15] Ren S, Chen J, Guo J, Liu Y, Xiong H, Jing B, et al. Exosomes from adipose stem cells promote diabetic wound healing through the eHSP90/LRP1/AKT Axis. Cells 2022;11(20). https://doi.org/10.3390/cells11203229.
[16] Familtseva A, Jeremic N, Tyagi SC. Exosomes: cell-created drug delivery systems. Mol Cell Biochem 2019;459(1–2):1–6. https://doi.org/10.1007/s11010-019-03545-4.
[17] Lee JH, Won YJ, Kim H, Choi M, Lee E, Ryoou B, et al. Adipose tissue-derived mesenchymal stem cell-derived exosomes promote wound healing and tissue regeneration. Int J Mol Sci 2023;24(13). https://doi.org/10.3390/ijms241310434.
[18] Livak KJ, Schmittgen TD. Analysis of relative gene expression data using real-time quantitative PCR and the 2(-Delta Delta C(T)) Method. Methods 2001;25(4):402–8. https://doi.org/10.1006/meth.2001.1262.
[19] Lee Jh WY, Kim H, Choi M, Lee E, Ryoou B, Lee SG, et al. Adipose tissue-derived mesenchymal stem cell-derived exosomes promote wound healing and tissue regeneration. Int J Mol Sci 2023;24(13):10434. https://doi.org/10.3390/ijms241310434.
[20] Puzar Dominkus P, Stenovec M, Sitar S, Lasic E, Zorec R, Plemenitas A, et al. PKH26 labeling of extracellular vesicles: characterization and cellular internalization of contaminating PKH26 nanoparticles. Biochim Biophys Acta Biomembr 2018;1860(6):1350–61. https://doi.org/10.1016/j.bbamem.2018.03.013.
[21] Huang J, Heng S, Zhang W, Liu Y, Xia T, Ji C, et al. Dermal extracellular matrix molecules in skin development, homeostasis, wound regeneration and diseases. Semin Cell Dev Biol 2022;128:137–44. https://doi.org/10.1016/j.semcdb.2022.02.027.
[22] Lin Z, Zhao C, Lei Z, Zhang Y, Huang R, Lin B, et al. Epidermal stem cells maintain stemness via a biomimetic micro/nanofiber scaffold that promotes wound healing by activating the Notch signaling pathway. Stem Cell Res Ther 2021;12(1):341. https://doi.org/10.1186/s13287-021-02418-2.
[23] Wu Y, Zhong JL, Hou N, Sun Y, Ma B, Nisar MF, et al. MicroRNA Let-7b inhibits keratinocyte migration in cutaneous wound healing by targeting IGF2BP2. Exp Dermatol 2017;26(2):116–23. https://doi.org/10.1111/exd.13164.
[24] Qian L, Pi L, Fang BR, Meng XX. Adipose mesenchymal stem cell-derived exosomes accelerate skin wound healing via the lncRNA H19/miR-19b/SOX9 axis. Lab Invest 2021;101(9):1254–66. https://doi.org/10.1038/s41374-021-00611-8.

[25] Wang LY, Zhang YT, Du LQ, Wu XY, Zhu J. The effect of SPARC on the proliferation and migration of limbal epithelial stem cells during the corneal epithelial wound healing. Stem Cell Dev 2021;30(6):301–8. https://doi.org/10.1089/scd.2020.0196.
[26] Adams JC. Matricellular proteins: functional insights from non-mammalian animal models. Curr Top Dev Biol 2018;130:39–105. https://doi.org/10.1016/bs.ctdb.2018.02.003.
[27] Huang H, Weng H, Sun W, Qin X, Shi H, Wu H, et al. Recognition of RNA N(6)-methyladenosine by IGF2BP proteins enhances mRNA stability and translation. Nat Cell Biol 2018;20(3):285–95. https://doi.org/10.1038/s41556-018-0045-z.
[28] Liu J, Yang Q, Sun H, Wang X, Saiyin H, Zhang H. The circ-AMOTL1/ENO1 Axis implicated in the tumorigenesis of OLP-associated oral squamous cell carcinoma. Cancer Manag Res 2020;12:7219–30. https://doi.org/10.2147/CMAR.S251348.
[29] Ou R, Lv J, Zhang Q, Lin F, Zhu L, Huang F, et al. circAMOTL1 motivates AMOTL1 expression to facilitate cervical cancer growth. Mol Ther Nucleic Acids 2020;19:50–60. https://doi.org/10.1016/j.omtn.2019.09.022.
[30] Yang Q, Du WW, Wu N, Yang W, Awan FM, Fang L, et al. A circular RNA promotes tumorigenesis by inducing c-myc nuclear translocation. Cell Death Differ 2017;24(9):1609–20. https://doi.org/10.1038/cdd.2017.86.
[31] Wang X, Ma R, Zhang X, Cui L, Ding Y, Shi W, et al. Crosstalk between N6-methyladenosine modification and circular RNAs: current understanding and future directions. Mol Cancer 2021;20(1):121. https://doi.org/10.1186/s12943-021-01415-6.
[32] Sun Y, Ju Y, Fang B. Exosomes from human adipose-derived mesenchymal stromal/stem cells accelerate angiogenesis in wound healing: implication of the EGR-1/lncRNA-SENCR/DKC1/VEGF-A axis. Hum Cell 2022;35(5):1375–90. https://doi.org/10.1007/s13577-022-00732-2.